PCCP

COMMUNICATION

View Article Online
View Journal | View Issue

Cite this: *Phys. Chem. Chem. Phys.*, 2014, **16**, 20415

Received 20th July 2014,
Accepted 20th August 2014

DOI: 10.1039/c4cp03210a

www.rsc.org/pccp

Monoclinic hafnium oxynitride supported on reduced graphene oxide to catalyse the oxygen reduction reaction in acidic media†

M. Chisaka,*[a] H. Sasaki[a] and H. Muramoto[b]

Monoclinic HfO_2 nanoparticles were doped with nitrogen *via* hydrothermal treatment that avoided high-cost pyrolysis with NH_3 gas in order to develop a novel oxygen reduction reaction catalyst for use in acidic media. Catalyst size reduction was achieved using a reduced graphene oxide support, and activity above 0.8 V was obtained.

Vehicles powered by polymer electrolyte fuel cells (PEFCs) are expected to be available in some markets as early as 2014. However, given the limited resource of platinum-group-metal (PGM) catalysts, the widespread use of these vehicles will only be practically viable upon reducing the amount of PGM catalysts within a single vehicle to below 10 g, comparable to that of conventional internal combustion vehicles.[1] Therefore, various types of non-PGM catalysts have been developed specifically for PEFC cathodes, as the slow kinetics of the oxygen reduction reaction (ORR) requires the use of one order of magnitude more PGM than in the corresponding anodes.[2] All current state-of-the-art non-PGM PEFC catalysts contain graphitized carbon materials such as carbon black,[3] carbonized polymers,[4] carbon nanotubes,[5] and ordered mesoporous carbon[6] that provide a conductive path to their active sites and/or help in forming those sites. Non-PGM catalyst loading in PEFC cathodes is large, typically several mg cm^{-2} or more, owing to limited activity in the acidic environment commonly found there. This results in a catalyst layer thickness of around 100 μm, more than one order of magnitude larger than that of conventional PGM catalysts. The application of backpressure is therefore needed[3,4,6] to improve oxygen diffusion in these thicker layers, which in turn increases system cost. Graphene is an ideal carbon material for non-PGM catalysts as it is composed of a single layer of graphite, thereby reducing both catalyst volume, and consequently, catalyst layer thickness. Therefore, graphene doped with non-metal elements such as nitrogen,[7] sulphur[8] and metal–graphene hybrids[9] has recently been investigated for its use as a non-PGM ORR catalyst in alkaline media. The use of graphene is not limited to fuel cell catalysts and is open for many other photochemical and electrochemical applications such as photocatalysts, solar cells, supercapacitors, batteries, and sensors. These backgrounds have been a strong motivation for the development of a graphene synthesis route, to date.[10]

Herein, we report a facile synthesis for the production of a new non-PGM catalyst composed of hafnium oxynitride supported on reduced graphene oxide (HfO_xN_y–rGO) and describe its activity in acidic media. HfO_xN_y was selected as an ORR catalyst because of its high stability in acidic media, as evidenced by its failure to dissolve in 0.1 mol dm^{-3} H_2SO_4 solution.[11] However, previous methods for synthesizing this catalyst supported on conventional carbon black (HfO_xN_y–C) use a two-step heating process that lasts at least four days and requires high-cost, high-purity NH_3 gas to successfully dope HfO_x with nitrogen in the second step. The synthetic method described herein relies on a one-pot synthesis of HfO_xN_y that does not require conventional treatment with NH_3. The GO sheet was selected as a graphene source because it contains a large number of oxygen functional groups which are favourable for the adsorption of the $Hf(OH)_4$ precursor. Additionally, new active sites for the ORR have been found.

HfO_xN_y–rGO synthesis began with the sonication of 10 cm^3 of an aqueous dispersion of GO (2 mg cm^{-3}, 763705, Sigma-Aldrich, U.S.) with 70 cm^3 of distilled water, after which the resulting dispersion was poured into a Teflon-lined autoclave and continuously stirred. Next, 0.76 g of $HfCl_4$ (Mitsuwa Chem. Co., Japan) was added to the dispersion; the resulting pH of 0.5–1 was then increased to a value greater than 8 through the slow addition of 59 cm^3 of a 0.5 mol dm^{-3} solution of NH_3, so as to effect complete hydrolysis of $HfCl_4$. The dispersion was then diluted with 40 cm^3 of ethanol, after which the autoclave was closed and the dispersion was subjected to hydrothermal

[a] *Department of Electronics and Information Technology, Hirosaki University, 3 Bunkyo-cho, Hirosaki, Aomori 036-8561, Japan. E-mail: chisaka@eit.hirosaki-u.ac.jp; Fax: +81 172 39 3559*

[b] *Cooperative Research Facility Center, Toyohashi University of Technology, 1-1 Hibarigaoka, Tempaku, Toyohashi, Aichi 441-8580, Japan*

† Electronic supplementary information (ESI) available: Mass activity *versus* potential curves, RRDE voltammograms, fitting results of a N 1s spectrum, C 1s spectra. See DOI: 10.1039/c4cp03210a

treatment for 6 h using a heating mantle set to temperatures T ranging from 384 to 463 ± 8 K. The dispersion was then allowed to cool, yielding grey-black coloured particles that were washed with distilled water until a neutral pH was obtained. The particles were then dried overnight at 380 K and placed in an alumina boat that was set in a horizontal quartz tube furnace, which was slowly evacuated and purged with N_2 gas. The catalyst particles were heated from room temperature to 1073 K at a rate of 500 K h^{-1} and were held at that temperature for 2 h, after which they were allowed to cool to room temperature. N_2 gas flow was set to 300 sccm (standard cubic centimetres per minute; 1 sccm = 1.67 × 10^{-8} m^3 s^{-1}) throughout pyrolysis. rGO sheets were synthesized under conditions identical to those for HfO_xN_y–rGO except for the addition of $HfCl_4$; in this case, hydrothermal treatment was carried out at 433 K.

The morphology of the catalysts was investigated using a field-emission transmission electron microscope (JEM-2100F, JEOL, Japan). The crystal structures of the catalysts were analysed using an X-ray diffractometer (M18XHF, Mac Science Co., Japan) equipped with a Cu-Kα radiation source generating at 50 kV and 30 mA. The scattering angle range of 5–80° was scanned at a rate of 2° min^{-1}. The chemical states of the catalysts were analysed using an X-ray photoelectron spectrometer (Quantera SXM, ULVAC-PHI, Inc., Japan) with an Al-Kα X-ray source (1486.6 eV).

Rotating disk electrode (RDE) voltammograms were obtained to help evaluate the ORR activity of the catalysts. The catalysts, 5% w/w Nafion solution (510211, Sigma-Aldrich, U.S.), and isopropyl alcohol were sonicated for 1200 s to obtain a catalyst ink with a catalyst mass fraction of 4.5% and a catalyst-to-Nafion mass ratio of 7/3. Several mm^3 aliquots were dropped onto glassy carbon (GC) disk electrodes with a diameter φ = 4 mm and air-dried at 320 K for at least 600 s. The dropping and drying procedure was repeated until the GC electrode was coated with the desired mass of the catalyst and Nafion, typically 0.3 mg; this value corresponds to a catalyst loading, m, of 2 mg cm^{-2}. Prior to this treatment, the surface of the GC disk electrodes was polished with 1.0 and 0.05 μm alumina slurries, washed with water, and then dried at 320 K in air. A conventional three-electrode cell was used, and electrochemical measurements were performed in 0.1 mol dm^{-3} H_2SO_4 at room temperature. The catalyst-coated GC disk electrode, a carbon paper electrode (TGP-H-120, Toray, Japan), and an Ag/AgCl (3 mol dm^{-3} NaCl) electrode (RE-1B, BAS Co., Japan) were used as the working, counter, and reference electrodes, respectively. The working electrode was set on a rotator (RRDE-3A, BAS Co., Japan). All working electrode potentials were referenced to a reversible hydrogen electrode (RHE). The RDE voltammograms were recorded using a potentiostat (Model 2323, BAS Co., Japan) by applying a disk potential, E, in the range of 0.11–1.26 V at a scan rate of 5 mV s^{-1} and a rotation speed of 1500 rpm after bubbling with O_2 and N_2 for 1800 s. The differences observed in the current per area between data obtained under a N_2 atmosphere (i_N) and that measured under an O_2 atmosphere (i_O) were assumed to correlate with the ORR.

Because both HfO_x particles and rGO sheets can be doped with nitrogen atoms, ORR activity of both HfO_xN_y–rGO and rGO sheets was compared to elucidate the origin of the ORR active sites in HfO_xN_y–rGO. Fig. 1(i) and (ii) show RDE voltammograms of rGO and HfO_xN_y–rGO, respectively. The background current (i_N) of rGO was more than ten times larger than that of HfO_xN_y–rGO, owing to the fact that HfO_xN_y–rGO contained only 4% w/w rGO. However, rGO showed an ORR current ($i_O - i_N$) at E of less than 0.6 V, which is more than 0.2 V lower than HfO_xN_y–rGO. Besides, rGO showed considerably low ORR current: $|i_O - i_N|$ for rGO was below $|i_N|$ even at the lowest E value of 0.11 V, as shown by the solid curve in Fig. 1(iii). In contrast, $|i_O - i_N|$ for HfO_xN_y–rGO was more than 10 times larger than $|i_N|$, as shown by the dashed curve.

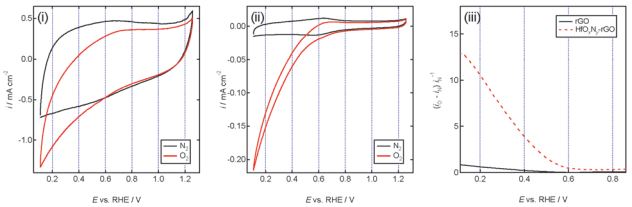

Fig. 1 RDE voltammograms of (i) rGO and (ii) HfO_xN_y–rGO hydrothermally synthesized at 433 K. Their normalized ORR current *versus* potential [$(i_O - i_N)\, i_N^{-1} - E$] curves are shown in (iii). Scans were performed under N_2 and O_2 with a rotation speed of 1500 rpm at a scan rate of 5 mV s^{-1} in 0.1 mol dm^{-3} H_2SO_4.

These results indicate that the ORR activity of HfO_xN_y–rGO originated from the HfO_xN_y particles, not from the rGO sheets. We therefore focus on the activity and properties of the HfO_xN_y particles hereafter.

Fig. 2 shows RDE voltammograms of five HfO_xN_y–rGO catalysts hydrothermally treated at various T before (left) and after (right) pyrolysis. All as-synthesized HfO_xN_y-rGO samples showed similarly poor activity, with $i_O - i_N$ having been observed at $E < 0.4$ V. Except for T = 384 K, activity was significantly enhanced by pyrolysis; interestingly, this enhancement was dependent solely on T and not on the pyrolysis temperature. Activity clearly increased with increasing T up to 453 K, but decreased at T exceeding that value. As shown in the inset, $i_O - i_N$ appeared at $E > 0.8$ V, a value comparable to that

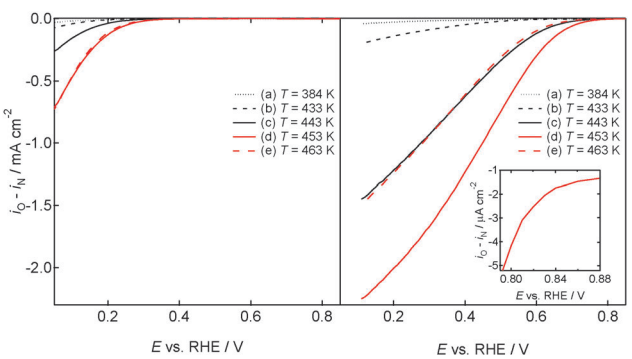

Fig. 2 RDE voltammograms of HfO_xN_y–rGO hydrothermally synthesized at (a) 384 K, (b) 433 K, (c) 443 K, (d) 453 K, and (e) 463 K, before (left) and after (right) pyrolysis. Experimental conditions were identical to those described in Fig. 1.

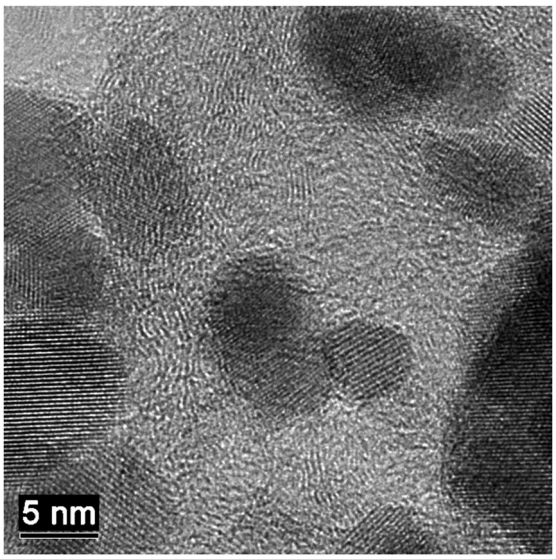

Fig. 3 An FE-TEM image of HfO_xN_y–rGO hydrothermally synthesized at 453 K.

of HfO_xN_y–C synthesized using conventional NH_3 treatment.[11–13] However, a limiting current density obtained from HfO_xN_y–rGO was only one third of that from HfO_xN_y–C whose HfO_xN_y particle size was approximately a few nanometres[12,13] indicating the lower active surface area due to the larger and non-uniform HfO_xN_y particles supported on rGO (Fig. 3, next section). Besides, the HfO_xN_y–rGO showed no plateau in Fig. 2. We previously reported that the Tafel slope decreased and thus the limiting current plateau appeared by reducing the HfO_xN_y particle size of HfO_xN_y–C owing to the change in the adsorption mechanism of oxygenated species.[13] Therefore, control of the HfO_xN_y particle size to a few nanometres is our next crucial research topic. Furthermore, note that no repeatable activity was observed for T = 384 K. Mass activity showed similar trends with T (S1, ESI†), indicating that the optimum T for HfO_xN_y activity is 453 K. The number of electrons transferred per unit oxygen molecule n on the surface of HfO_xN_y–rGO which showed the maximum activity was 3.4 at E = 0.6 V (S2, ESI†) indicating that ORR proceeded *via* both 2- ($O_2 + 2H^+ + 2e^- \rightarrow H_2O_2$) and 4-electron reaction ($O_2 + 4H^+ + 4e^- \rightarrow 2H_2O$) pathways. The n value is lower than that for previously reported HfO_xN_y–C whose synthesis route has been optimized.[13] Because H_2O_2 should degrade the proton-conductive perfluorosulfonate-ionomer (PFSI) in catalyst layers and PFSI membranes of PEFCs,[14] the formation should be suppressed and therefore the n value should be increased by, for example, changing the synthesis conditions.[15] To reveal the factors affecting ORR activity observed only after pyrolysis, some physical and chemical properties were investigated.

Fig. 3 shows a field-emission transmission electron microscopy (FE-TEM) image of the T = 453 K HfO_xN_y–rGO sample after having been subjected to pyrolysis; recall that this is the sample which showed the maximum activity. Crystallized black/dark-grey HfO_xN_y particles with non-uniform sizes are seen supported on light-grey rGO sheets. Some of the particles, including those shown in the centre of the image, are several nanometres in diameter, whereas other particles, including those shown on the right and left sides of the image, formed aggregates with diameter on the order of several tens of nanometres, indicating that some synthetic parameters, such as the mass ratio of HfO_xN_y to rGO, still need to be optimized to elicit uniform size and to increase ORR currents.

Fig. 4 shows X-ray diffraction (XRD) patterns of HfO_xN_y–rGO at five different T values before (left) and after (right) pyrolysis. No sharp peaks were observed at T = 384 K; however, at T = 433 K, weak peaks assigned to a monoclinic HfO_2 phase appeared, indicating the hydrolysis of $HfCl_4$. These peaks sharpened upon increasing T up to 453 K, and remained effectively identical up to T = 463 K, suggesting an increase in HfO_2 crystallinity and/or grain size. Pyrolysis sharpened all the peaks while still retaining the previously observed trend.

The bonding states of the HfO_xN_y surface were investigated next using X-ray photoelectron spectroscopy (XPS), seeing how the ORR is a surface phenomenon. Hf 4f and N 1s spectra of all HfO_xN_y–rGO samples, both from before and after pyrolysis, are shown in Fig. 5. The O 1s spectra were not used in this study because of the contribution from functional groups on the rGO surface. It is well known that the Hf 4f level is spin–orbit split into Hf $4f_{7/2}$ and Hf $4f_{5/2}$ sublevels, which can be seen as a doublet in Hf 4f spectra.[16] Except for T = 463 K, pyrolysis did not significantly change the appearance of the Hf 4f spectra. The T = 384 K HfO_xN_y–rGO sample showed two peaks at approximately 17.4 and 18.8 eV after pyrolysis, typical for Hf^{4+} in HfO_2.[16] These peaks shifted to higher binding energies with increasing T up to 453 K, indicative of the incorporation of charged oxygen defects,[17] but then decreased for T = 463 K. Weak but apparent peaks assigned to Hf–N bonding at approximately 396 eV[18] and C–N bonding at approximately 398–402 eV[18,19] were observed in the N 1s spectra, indicating that small amounts of nitrogen atoms were successfully introduced into both the HfO_x particles and the rGO sheets during hydrothermal treatment. The nitrogen-doping level on the surface of the HfO_xN_y particle is quite low; one order of magnitude lower than that observed from

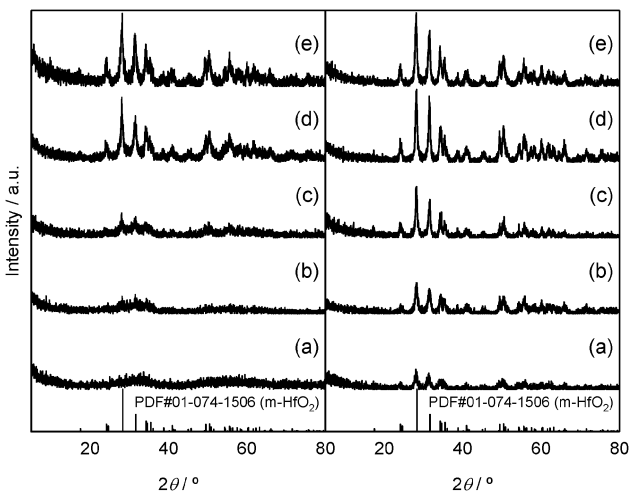

Fig. 4 XRD patterns of HfO_xN_y–rGO hydrothermally synthesized at (a) 384 K, (b) 433 K, (c) 443 K, (d) 453 K, and (e) 463 K, before (left) and after (right) pyrolysis.

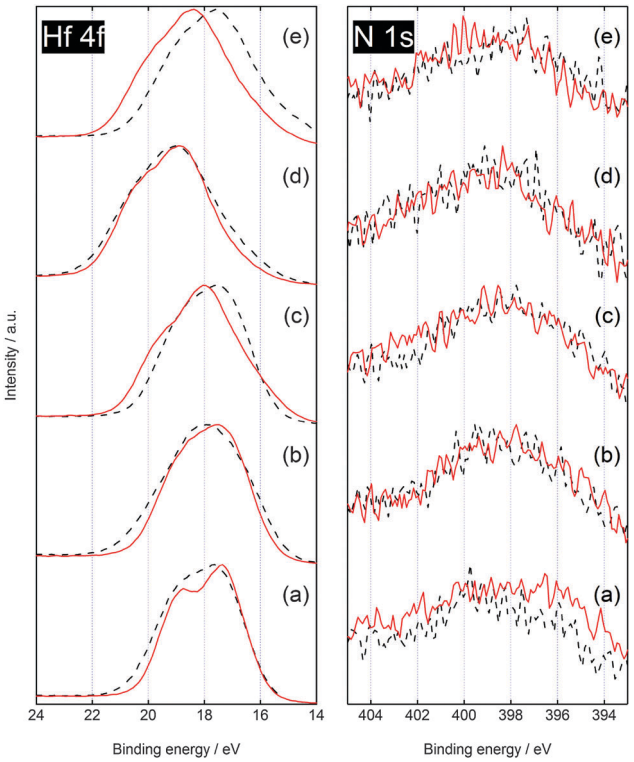

Fig. 5 (Left) Hf 4f and (right) N 1s spectra of HfO_xN_y–rGO hydrothermally synthesized at (a) 384 K, (b) 433 K, (c) 443 K, (d) 453 K, and (e) 463 K before (dashed line) and after (solid line) pyrolysis.

our previous study using NH_3-gas pyrolysis[11] (S3, ESI†). However, the fact that the spectra did not change as a result of pyrolysis reveals that these nitrogen atoms were stable in both the HfO_2 and the graphitic lattice. The extent of doping as well as the binding energy was almost constant with increasing T, indicating that the observed change in the Hf 4f binding energy was not from Hf–N bonding, but rather from oxygen defects.

These results demonstrate that both ORR activity and the number of oxygen defects in monoclinic HfO_2 showed a volcano-type dependence on T with an optimum value of 353 K, suggesting that oxygen defects form at the active sites. Anion defect sites have been suggested as active towards the ORR in other oxide,[20] oxynitride,[12] and nitride[21] catalysts; however, nitrogen-free monoclinic HfO_2 exhibiting oxygen defects showed poor activity in a previous study,[13] with this being the first to show ORR activity with an onset potential higher than 0.8 V for nitrogen-doped monoclinic HfO_2. Initial pH treatment allowed the $HfCl_4$ precursor to fully hydrolyse to $Hf(OH)_4$. For subsequent hydrothermal treatments at $T \geq 433$ K, both monoclinic HfO_2 crystallization and nitrogen doping proceeded simultaneously. Besides, reduction of GO sheets proceeded at this T range (S4, ESI†), suggesting that the electronic conductivity increased and thereby the ORR activity of HfO_xN_y particles was enhanced. However, when T increased to 463 K, the number of oxygen defects decreased, while N_2 pyrolysis did not allow a recovery of these defects to the point observed in the T = 453 K sample. Although the precise mechanism for the decrease in Hf 4f binding energy and the number of oxygen defects that were observed from T = 453 K to T = 463 K is not currently clear, it may in part be attributed to the reaction of functional group oxygen atoms on the GO sheets and HfO_x particles that occurs at high T values, as is observed in the case of TiO_x–rGO nanocomposite dye-sensitized solar cells.[22]

Conclusions

A new active site for ORR in nitrogen-doped monoclinic HfO_2 was found in this study. The developed hydrothermal synthesis route dramatically shortened the synthesis time while retaining the ORR activity when compared with the cubic Hf_2ON_2 phase in our previous HfO_xN_y–C catalysts.[11–13] Both the synthetic cost and catalyst volume were significantly reduced by changing from a conventional carbon black support to rGO and by using an NH_3 solution and hydrothermal treatment instead of relying on the previous method of pyrolysis using high-purity NH_3 gas. Maximum ORR activity was obtained at above 0.8 V; however, further enhancement is necessary if this system is to be used in practical applications. This activity enhancement could be achieved by reduction of the HfO_xN_y particle size and optimization of the nitrogen doping level and the number of defects.

Acknowledgements

This work was partially supported by an Adaptable and Seamless Technology Transfer Program through target-driven R&D, AS242Z00224L, from the Japan Science and Technology Agency.

Notes and references

1 B. G. Pollet, I. Staffell and J. L. Shang, *Electrochim. Acta*, 2012, **84**, 235.
2 H. A. Gasteiger, J. E. Panels and S. G. Yan, *J. Power Sources*, 2004, **127**, 162.
3 G. Wu, K. L. More, C. M. Johnston and P. Zelenay, *Science*, 2011, **332**, 443.
4 E. Proietti, F. Jaouen, M. Lefèvre, N. Larouche, J. Tian, J. Herranz and J. P. Dodelet, *Nat. Commun.*, 2011, **2**, 416.
5 Y. Li, W. Zhou, H. Wang, L. Xie, Y. Liang, F. Wei, J. C. Idrobo, S. J. Pennycook and H. Dai, *Nat. Nanotechnol.*, 2012, **7**, 394.
6 J. Y. Cheon, T. Kim, Y. M. Choi, H. Y. Jeong, M. G. Kim, Y. J. Sa, J. Kim, Z. Lee, T. H. Yang, K. Kwon, O. Terasaki, G. G. Park, R. R. Adzic and S. H. Joo, *Sci. Rep.*, 2013, **3**, 2715.
7 L. Qu, Y. Liu, J. B. Baek and L. Dai, *ACS Nano*, 2010, **4**, 1321.
8 Z. Sofer, O. Jankovský, P. Šimek, K. Klímová, A. Macková and M. Pumera, *ACS Nano*, 2014, **8**, 7106.
9 H. L. Poh, P. Šimek, Z. Sofer and M. Pumera, *ACS Nano*, 2013, **7**, 5262.
10 H. L. Poh, Z. Sofer, J. Luxa and M. Pumera, *Small*, 2014, **10**, 1529.
11 M. Chisaka, T. Iijima, T. Yaguchi and Y. Sakurai, *Electrochim. Acta*, 2011, **56**, 4581.
12 M. Chisaka, Y. Suzuki, T. Iijima and Y. Sakurai, *J. Phys. Chem. C*, 2011, **115**, 20610.

13 M. Chisaka, Y. Suzuki, T. Iijima, Y. Ishihara, R. Inada and Y. Sakurai, *ECS Electrochem. Lett.*, 2012, **1**, F4.
14 S. Hommura, K. Kawahara, T. Shimohira and Y. Teraoka, *J. Electrochem. Soc.*, 2008, **155**, A29.
15 M. Chisaka and H. Muramoto, *ECS Electrochem. Lett.*, 2014, **3**, F1.
16 S. Hofmann and J. M. Sanz, *J. Trace Microprobe Tech.*, 1982, **1**, 213.
17 M. Copel, R. P. Pezzi, D. Neumayer and P. Jamison, *Appl. Phys. Lett.*, 2006, **88**, 072914.
18 M. Lee, Z. H. Lu, W. T. Ng, D. Landheer, X. Wu and S. Moisa, *Appl. Phys. Lett.*, 2003, **83**, 2638.
19 J. R. Pels, F. Kapteijn, J. A. Moulijn, Q. Zhu and K. M. Thomas, *Carbon*, 1995, **33**, 1641.
20 A. Ishihara, M. Tamura, Y. Ohgi, M. Matsumoto, K. Matsuzawa, S. Mitsushima, H. Imai and K. Ota, *J. Phys. Chem. C*, 2013, **117**, 18837.
21 H. Zhong, H. Zhang, G. Liu, Y. Liang, J. Hu and B. Yi, *Electrochem. Commun.*, 2006, **8**, 707.
22 T. T. Wu and J. M. Ting, *Int. J. Energy Res.*, 2014, **38**, 1438.